

SCIENTIFIC REPORTS



OPEN

Bacteriophage T5 gene D10 encodes a branch-migration protein

Io Nam Wong^{1,2}, Jon R. Sayers^{2,3} & Cyril M. Sanders^{1,3}

Received: 29 July 2016

Accepted: 22 November 2016

Published: 23 December 2016

Helicases catalyze the unwinding of double-stranded nucleic acids where structure and phosphate backbone contacts, rather than nucleobase sequence, usually determines substrate specificity. We have expressed and purified a putative helicase encoded by the D10 gene of bacteriophage T5. Here we report that this hitherto uncharacterized protein possesses branch migration and DNA unwinding activity. The initiation of substrate unwinding showed some sequence dependency, while DNA binding and DNA-dependent ATPase activity did not. DNA footprinting and purine-base interference assays demonstrated that D10 engages these substrates with a defined polarity that may be established by protein-nucleobase contacts. Bioinformatic analysis of the nucleotide databases revealed genes predicted to encode proteins related to D10 in archaeobacteria, bacteriophages and in viruses known to infect a range of eukaryotic organisms.

Helicases play central roles in DNA replication ensuring fidelity¹. Although a single replicative helicase may be responsible for unwinding the majority of a dsDNA genome, auxiliary helicases are necessary for replication re-start, DNA repair and recombination. Problems such as fork collapse or stalling at DNA lesions are likely to be routine occurrences during replication cycles, especially in organisms with large genomes. In *E. coli*, it has been estimated that up to 50% of initiation events from *oriC* may fail and lead to replication forks that must be re-activated independently of the normal initiation process². The pathways that restore the replication fork and repair damage cope with a variety of DNA structures and often involve homologous genetic recombination. Accordingly, many helicases participating in DNA damage response pathways, including those with branch migration activity, are highly DNA structure-specific and it is this, rather than nucleotide sequence, that determines where and how they act on DNA^{1,3}. Nevertheless, the unifying biochemical feature of all helicases is that energy from nucleotide hydrolysis is coupled to translocation and base-pair separation. Overall, this process is unbiased by nucleic acid sequence, consistent with structural and biochemical studies that show helicases interacting with nucleic acids principally via phosphodiester backbone contacts^{4–6}.

DNA structure-specific helicases also regulate replication origins and this is best understood in bacteriophage systems. For example, bacteriophage T4 has two modes of replication initiation^{7–10}. One is origin-dependent and depends on the 5′–3′, hexameric helicase T4 gp41 at the early stage of infection^{11,12}. In order to accelerate the speed of replication and increase the burst size, a recombination-dependent replication (RDR) mode becomes predominant late in T4 infection. Here, products from the early origin-dependent DNA replication can invade each other by homologous recombination to generate D-loops for initiation of RDR^{8,9} and this requires the helicase activity of UvsW which promotes branch migration to stabilise the D-loop. UvsW also participates in the reactivation of stalled replication forks and branch migration of Holliday junctions^{13–15}. Although best characterised in bacteriophage, RDR is not limited to prokaryotes and has been observed in mammalian viruses including HSV1 and papillomavirus¹⁶.

T5 is a lytic bacteriophage of *E. coli*^{17,18} that has a highly efficient replication cycle^{19–22}. To date, only three proteins, D9 polymerase, D15 flap endonuclease and helicase D2 have been identified as replication enzymes in this bacteriophage^{23–26}. Here we present biochemical analyses of a second bacteriophage T5 helicase, the D10 gene product²⁷. The closest D10 protein homologs were identified as the *Archeoglobus* Xpb helicase, whose homologs have roles in transcription-coupled repair and nucleotide excision repair, and the UvsW protein encoded by bacteriophage T4. Additionally, homologs of the D10 protein were also found encoded within the genomes of several viruses capable of infecting single and multi-cellular eukaryotic organisms. We present biochemical

¹Department of Oncology & Metabolism, University of Sheffield Medical School, Beech Hill Rd, Sheffield, S10 2RX, UK. ²Department of Infection, Immunity & Cardiovascular Disease, University of Sheffield Medical School, Beech Hill Rd, Sheffield, S10 2RX, UK. ³Sheffield Institute for Nucleic Acids, University of Sheffield Medical School, Beech Hill Rd, Sheffield, S10 2RX, UK. Correspondence and requests for materials should be addressed to J.R.S. (email: j.r.sayers@sheffield.ac.uk) or C.M.S. (email: c.m.sanders@sheffield.ac.uk)

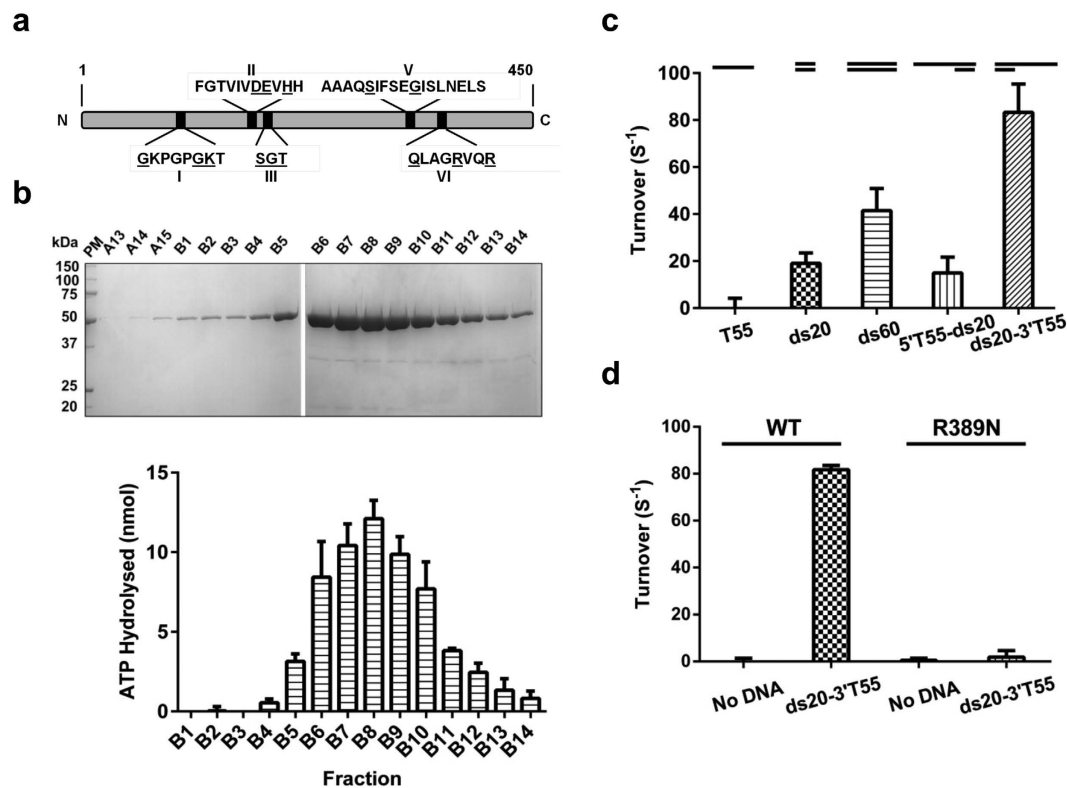


Figure 1. Conserved T5 D10 helicase motifs and ATPase activity of purified protein. (a) Location of five conserved SF2 helicase motifs (I, II, III, V, VI) identified in D10. (b) Fractions containing D10 protein eluted from the final Superdex 75 SEC column analysed by SDS-PAGE (upper) and ATPase activity of corresponding D10 peak fractions measured in the presence of DNA substrate ds20-3'T55 (20 bp dsDNA and a 3' 55-base oligo-dT overhang, lower panel). (c) ATPase activity of D10 (5 nM) determined in the presence of DNA substrates (5 nM): ssDNA, dsDNA and partial duplexes with a 20 bp and either a 5' or 3' 55 oligo-dT overhang (three repeats, mean and SD). (d) ATPase activities of wild-type D10 and R389N (5 nM) determined in the absence or presence of 5 nM ds20-3'T55 (three repeats, mean and SD).

studies showing that the D10 protein catalyses branch-migration *in vitro* and unwinds three- and four-strand DNA structures resembling DNA replication, recombination and repair intermediates. Intriguingly, unwinding of branched dsDNA structures by the D10 protein is highly sequence dependent and sensitive to purine modification interference, while DNA binding and DNA-dependent ATPase activity are largely sequence independent. To our knowledge this is the first time that nucleobase sequence has been shown to influence unwinding by a DNA helicase and branch migration protein.

Results

Sequence analysis. An analysis of the amino acid sequence of D10 revealed five conserved helicase motifs (Fig. 1a) belonging to the helicase superfamily 2 (SF2), including three universal helicase motifs, Walker A (motif I), Walker B (motif II) and an arginine finger (motif VI)¹. Furthermore, we identified Xpb and UvsW helicases from *Archaeoglobus fulgidus* and bacteriophage T4 respectively, to be the closest characterised homologs of D10 (Supplementary Figure S1a). The D10 protein exhibits 20–30% identity (40–45% similarity) with the *A. fulgidus* Xpb and UvsW proteins including conserved helicase motifs and a basic/aromatic loop implicated in nucleic acid binding²⁸. Intriguingly, aside from the expected orthologs and uncharacterised homologs present in T5-like bacteriophages, our analyses identified proteins encoded in the genomes of a number of viruses capable of infecting eukaryotic organisms as the closest homologs of the D10 protein. These included: Chorella and Marma viruses infecting the protozoans *Paramecium* and *Acanthamoeba* respectively; the Insectomime and *Armadillidium vulgare* iridescent viruses that infect insects; and the Singapore grouper iridovirus (Supplementary Figure S1b). A structural model of the D10 protein (Supplementary Figure S2) shows that the residues identified in the sequence alignments are present both in the core of the enzyme as well as the extended protein fold (Supplementary Figure S1b, and Video).

Purification of T5 D10. The D10 helicase and a variant (R389N) were expressed in recombinant *E. coli* and purified by affinity, ion exchange and size exclusion chromatography (SEC), yielding approximately 0.01 and 0.06 mg of wild type D10 and D10 R389N protein respectively per gram of cells. Elution from the SEC column was consistent with a monomeric 50 kDa molecule and protein fractions contained a DNA-dependent ATPase activity (Fig. 1b). This enzymatic activity corresponded exactly with the protein concentration of the fractions.

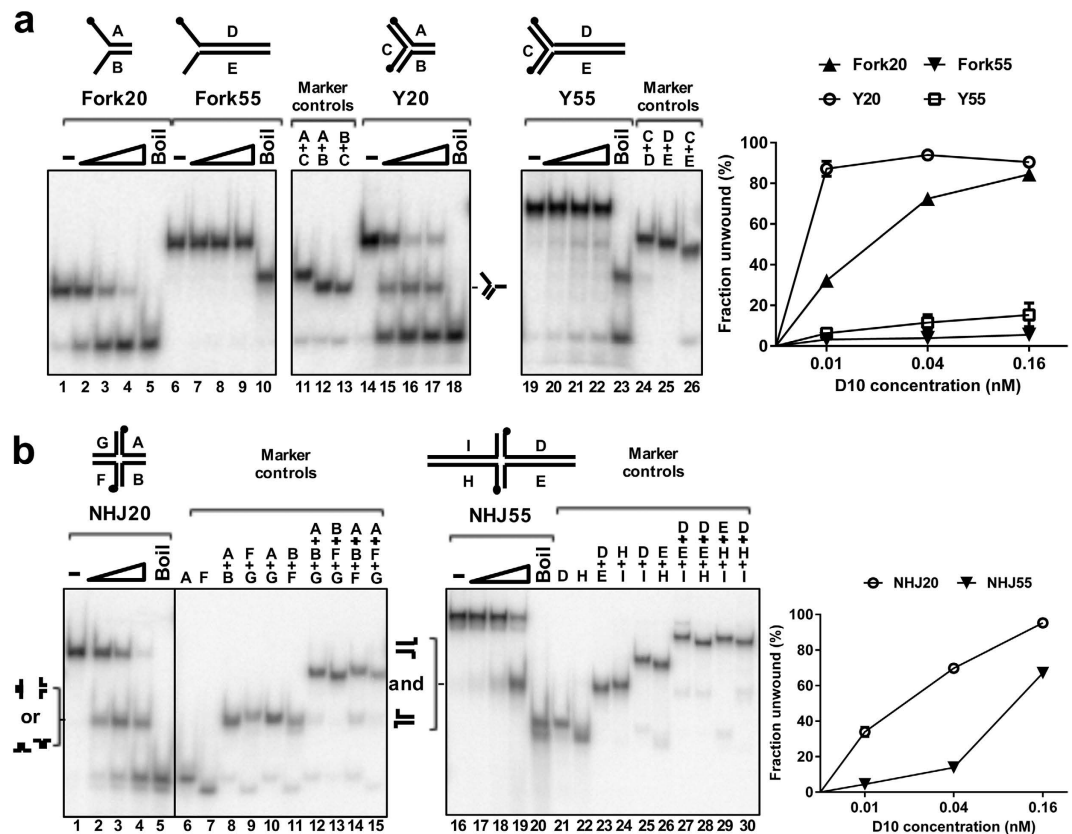


Figure 2. D10 unwinding of three- and four-way junction DNA. Substrates (0.1 nM) ^{32}P end-labelled as indicated (black circles). (a) Unwinding of Y-shaped DNA molecules (0.01, 0.04 and 0.16 nM D10). Lanes 1, 6, 14 and 19, no protein/native substrates (-) and 5, 10, 18 and 23 show denatured controls (boil), as indicated in all subsequent Figures. Lanes 11–13 and 24–26 are markers of possible products. The graph on the right shows quantitative data for D10 unwinding (three repeats, mean and SD, standard deviation). (b) Unwinding of four-way (cruciform) DNA structures NHJ20 and NHJ55. Native and heat denatured substrates are indicated (lanes 1 and 16, 5 and 20) and lanes 6–15 and 21–30 are marker lanes for all possible products. Quantified data are shown in the graph on the right (3 repeats, mean and SD).

Initial investigations with various linear DNA substrates including ssDNA (T55), blunt-ended dsDNA (20 and 60 bp), and partially single- and double-stranded molecules (ss-dsDNA) with either 5' or 3' ssDNA overhangs (20 bp and T55 ssDNA), demonstrated that only substrates with a duplex DNA component stimulated D10 ATPase activity. Also, the substrate with 20 bp of dsDNA and a T55 3' overhang (ds20-3'T55) was the most potent stimulator of ATPase activity (Fig. 1c). We also attempted to obtain D10 proteins with alterations in the three conserved motifs I, II and VI. However, despite successful cloning, only D10-R389N (motif VI) was successfully expressed and purified. ATPase activity was almost completely abolished by the point mutation resulting in a substitution (R389N) in the conserved arginine finger motif (Fig. 1d), confirming that the DNA-dependent ATPase activity is attributable to the D10 wild type protein.

D10 Unwinds branched DNA substrates. Even though the ATPase activity of D10 was stimulated by ss-dsDNA substrates they were not unwound, nor could we detect a strand annealing activity for D10 that could confound interpretation of these results (Supplementary Figure S3 and Fig. 4a below). Since D10 shares sequence similarity with T4 UvsW, we considered whether D10 could, like UvsW¹⁵, unwind more complex branched DNA substrates with ss- and dsDNA arms (fork-like molecules/Y-junctions). D10 efficiently unwound a 20-bp duplex with two 20-base ssDNA arms (Fig. 2a, substrate Fork20), but not a similar molecule with the duplex arm extended to 55 bp by increasing the length of oligonucleotides A and B, even at the highest concentrations of protein tested (Fig. 2a, substrate Fork55). Similarly, a dsDNA Y-junction with three 20-bp duplex arms was unwound efficiently, but not the substrate with one dsDNA arm extended to 55 bp (Fig. 2a, substrates Y20, and Y55, respectively). Both of these substrates, Fork20 and Y20, were only unwound by D10 in the presence of ATP (Supplementary Figure S4). In addition, for Y20, D10 preferentially dissociated only one of the three strands (oligo A) from the substrate, as described in further detail below. Thus, unlike UvsW, D10 can unwind DNA Y-junctions, although the length of the dsDNA substrate appears to impose limits on the ability of D10 to unwind certain structures *in vitro*.

Next, we tested the ability of the D10 protein to unwind synthetic cruciform (four-way) non-homologous Holliday junction substrates, as these are unwound by T4 UvsW. Substrate NHJ20, with four 20 bp non-homologous dsDNA arms, was unwound generating two sets of products, forked DNA and ssDNA (Fig. 2b).

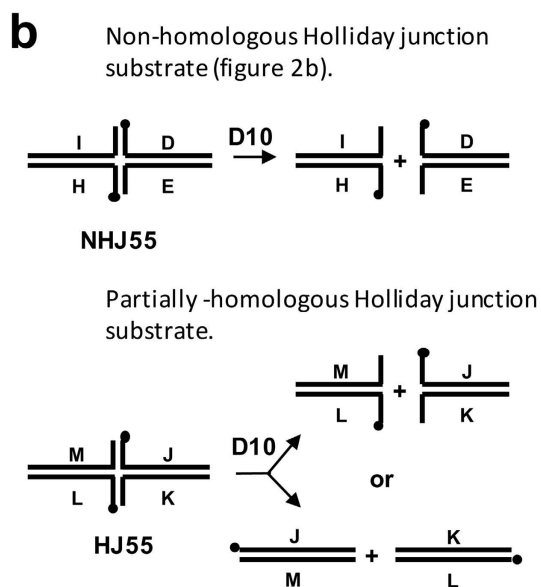
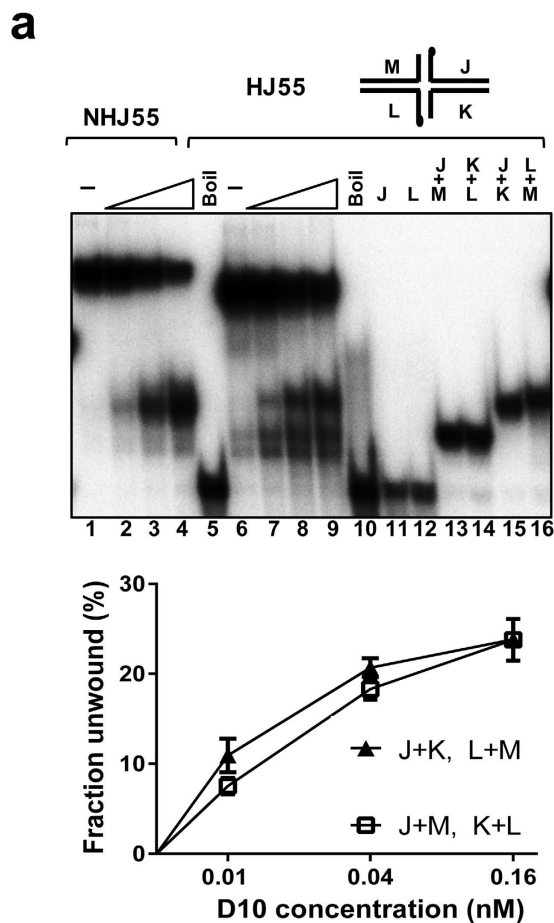


Figure 3. D10 Unwinding of a partially homologous Holliday junction substrate. (a) Substrate HJ55 (0.1 nM) was unwound by D10 (0.01, 0.04 and 0.16 nM, lanes 7–9) resulting in two kinds of products, fork DNA and recombined duplex DNA, identified from marker lanes 11–16. Lanes 1–5 show the unwinding and control reactions for the substrate NHJ55 run in parallel where only one class of product was observed as demonstrated in Figure 2. The graph below gives the percentage of each product class. (b) Schematic representation for D10 unwinding of non-homologous (NHJ55) and partially-homologous (HJ55) substrates.

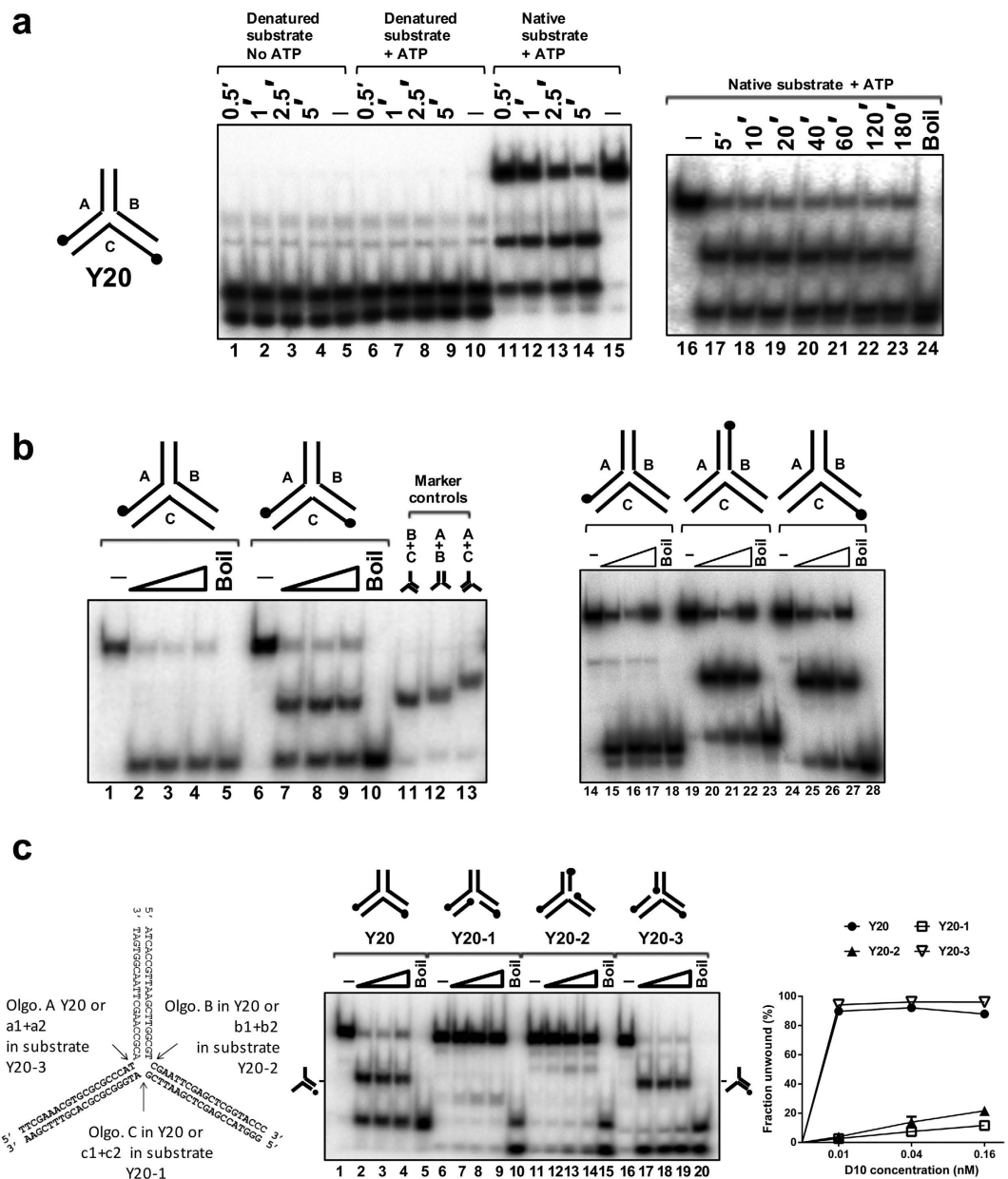


Figure 4. D10 processing of substrate Y20. (a) Time-course for unwinding of Y20 (0.1 nM) with oligonucleotides A and C ³²P end-labeled. Analyzed in lanes 1–10 are reaction products where substrate Y20 was heat denatured before addition to the reactions. D10 failed to catalyze strand annealing with or without ATP present, as indicated. Lanes 11 to 15 show accumulation of unwinding products of native Y20 substrate in parallel reactions with ATP sampled in a 5 minute time frame (0.1 nM substrate, 0.04 nM D10). Lanes 5, 10 and 15 are no protein controls. Lanes 16 to 24 show product accumulation over an extended time frame up to 180 minutes. (b) Helicase reactions showing preferential displacement of oligonucleotide A from substrate Y20. Lanes 1–13, helicase reactions with Y20 (0.1 nM) radiolabelled on strand A only or strands A and C, demonstrating that oligonucleotide A is preferentially displaced. Lanes 1 and 6, no protein control (-); lanes 5 and 10, heat-denatured substrate control (Boil); lanes 2–4 and lanes 7–9, with D10 (0.01, 0.04 and 0.16 nM); lanes 11–13, markers for possible products. Lanes 14–28 helicase reactions performed with separately labeled oligonucleotides A, B and C under the same conditions. (c) Processing of Y20 substrates with a nick positioned in each of the oligonucleotide as illustrated on the left. Centre, helicase reactions (0.1 nM substrate, 0.01, 0.04, 0.16 nM D10) for substrates Y20, Y20-1, Y20-2 and Y20-3 with the labelled oligonucleotides indicated for each substrate (black circle). Statistical data (three repeats, mean and SD) are shown in the graph on the right.

However, unwinding of the substrate NHJ55 with two 55 bp and two 20 bp dsDNA arms generated only one kind of product, a forked DNA with only a 55 bp dsDNA arm (Fig. 2b). Furthermore, the D10 ATPase-deficient variant

R389N failed to unwind NHJ20 but retained equivalent DNA binding activity to wild type, confirming that the observed reaction products result from the enzymatic action of D10 (Supplementary Figure S5).

As mentioned above, one feature of our observations was that dsDNA length appears to impose a restriction on the ability of D10 to unwind certain test substrates (Fig. 2a). One possibility is that the enzyme can only melt ≤ 20 bp of duplex DNA at, or close to, the substrate junction point. Alternatively, the longer DNA arms could re-anneal before completely dissociated or, envisioning a branch migration activity, the non-homologous nature of the test substrate could restrict the length of dsDNA that can be unwound. To investigate these possibilities, we constructed a close mimic of a natural Holliday junction substrate, consisting of a pair of long (55 bp) homologous duplex arms and a pair of short (20 bp) heterologous duplex arms (substrate HJ55, Fig. 3). In comparison to NHJ55, D10 converted HJ55 with two homologous 55-base-pair dsDNA arms into two different kinds of products; fork DNA and recombined linear duplex DNA (Fig. 3a), resulting from unwinding of HJ55 in either of two possible orientations. D10 therefore has branch-migration activity and can unwind DNA lengths greater than 55 base pairs.

DNA Sequence context and unwinding activity of D10. The data described above identified three- and four-way branched DNA structures, as substrates for the D10 helicase and indicated that D10 has branch migration activity. However, these data also show that D10 unwinding action is influenced by additional parameters other than DNA structure and length. For example, D10 could completely dissociate the substrate Fork20 with a 20 bp duplex and two 20 base ssDNA arms (Fig. 2a). It could also displace a 40 base oligonucleotide from substrate Y20 with three 20 bp duplex DNA arms (Fig. 2a), but the co-product that resembles Fork20 (20 bp and two 20 base ssDNA arms) was only poorly unwound, even in an extended time course (Fig. 4a). Furthermore, the relative mobility of the unwinding products indicated that there was a very strong bias as to which 40 base oligonucleotide was displaced from the Y20 substrate (Fig. 2a, lanes 11–13 compared to 15–17), which we unambiguously identified as oligonucleotide A (Fig. 4b). There are two possibilities for interpreting these data: either DNA sequence or secondary structure formed by ssDNA arms can influence D10 unwinding activity.

In order to minimize undesirable secondary structure and further explore the potential sequence selectivity of DNA unwinding in the D10 enzyme, the substrate Y20 was compared to the same substrates but with a nick at one of the three junction branch points in each substrate (Fig. 4c). According to Sabir and co-workers, all these three nicked substrates should have the same fully complementary largely symmetrical conformation without coaxial stacking of arms²⁹. Thus, we expected all the nicked Y-junctions to be unwound to similar extents. Surprisingly however, as shown in the electrophoretogram in Fig. 4c, compared to Y20, only Y20-3 (oligo A nicked) was unwound efficiently. As summarised graphically (Fig. 4c), practically all of substrates Y20 and Y20-3 were unwound at the lowest protein concentration tested, but the extents of unwinding of Y20-1 and Y20-2 were at least 20 fold lower. The reaction products of Y20 and Y20-3 were also both consistent with displacement of the sequences corresponding to oligonucleotide A; two oligonucleotides in the case of substrate Y20-3 (a1 and a2). However, although poorly unwound, the reaction products of Y20-1 and Y20-2 were not consistent with preferential displacement of this sequence (Fig. 4c and Supplementary Figure S6a).

To further explore the basis of this substrate-specific DNA unwinding we tested whether the various Y-junctions differed in their binding affinity for the D10 protein and whether they could stimulate DNA-dependent ATPase activity. Substrates Y20, Y20-1 and Y20-2 showed little detectable difference in their binding affinities for D10, while Y20-3 (oligonucleotide A nicked) showed a modest decrease in affinity (~ 2 fold) as judged by the sensitivity of substrate binding to the addition of non-specific competitor DNA in the reaction (Supplementary Figure S6b). Furthermore, all Y-junctions with and without nicks stimulated the DNA-dependent ATPase activity of D10 to similar extents (Supplementary Figure S6d). Thus, displacement of oligonucleotides A or a1 and a2 from Y20 is dependent on the strand continuity of oligonucleotides B and C, indicating a precise orientation of D10-substrate unwinding relative to DNA sequence.

High-resolution footprinting of D10 bound to a dsDNA Y-junction. Next, we performed high-resolution hydroxyl radical (OH \cdot) footprinting to investigate the binding of D10 to substrate Y20. Three D10 binding reactions, each with a different strand of Y-20 labelled, were assembled and the OH \cdot was generated by Fenton's reaction. After limited cleavage, the DNA products were recovered, separated on a sequencing gel analysed by quantitative phosphorimaging. D10 protected the 23–30 bases, approximately centred around the junction point in each DNA strand of Y20 (Fig. 5a).

An analysis of the protection pattern with increasing protein concentration (Fig. 5b) suggested that protein binding to the Y-junction was progressive, without demonstrating a significant bias for any strand or arm of the substrate. However, although the Y-junction substrate has trilateral symmetry the protection pattern, summarised in Fig. 5c, did not display such symmetry, with the length of DNA protected on oligonucleotide C (30 nt.) more extensive than that of A (26 nt.) or B (23 nt.).

DEPC Interference analysis of D10-Y20 DNA unwinding reactions. Diethyl pyrocarbonate (DEPC) carbethoxylates N7 of purines and the presence of this adduct can interfere with close protein-DNA base contacts required for substrate unwinding³⁰. Y20 substrates were generated with one strand end-labelled with ³²P and modified with DEPC and used in unwinding reactions. After electrophoresis, the intact substrate and product were recovered, cleaved with piperidine and analysed on a sequencing gel (Fig. 6a), as above. Carbethoxylation of several purine residues on each strand inhibited unwinding (Fig. 6b). Quantification of the data revealed that the number of purines and the magnitude of the resulting effects of DEPC modification on inhibition of unwinding are far greater for oligonucleotides B and C, compared to the displaced oligonucleotide A, where they are also present exclusively on the 5' half of oligonucleotide A. Furthermore, the three purines at or close to the junction

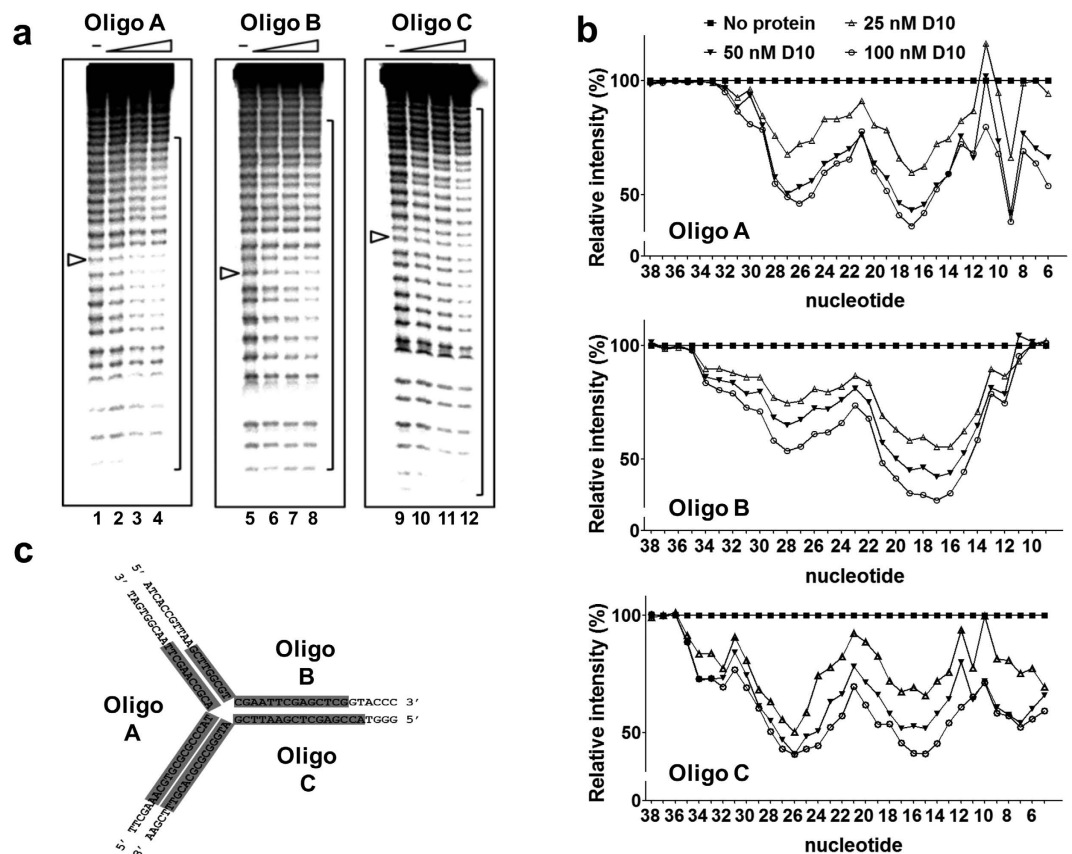


Figure 5. Hydroxyl radical footprinting of the D10-Y20 DNA complex. (a) Either oligonucleotide A, B or C of the Y20 substrate was ^{32}P end-labelled. Binding reactions contained 10 nM substrate and 0, 25, 50, 100 nM D10. The 20th nucleotide at the branch point of each strand are indicated by arrows. (b) Regions of protection were determined by comparing densitometric tracings with and without D10 at the indicated protein concentrations. For each nucleotide position, the intensity of each band was compared directly to the intensity of the reaction with no protein (100% intensity) to give the relative intensity of protection as a function of increasing protein concentration. (c) The regions of protection are schematically represented on the Y20 sequence.

point of oligonucleotide A (indicated with arrows in Fig. 6c) do not alter the efficiency of the unwinding reaction when carboxylated, while the purines in similar positions in oligonucleotide B and C show significant effects on unwinding when modified. These data imply that base (purine) contacts in oligonucleotide B and C, particularly those close to the junction point, influence the displacement of oligonucleotide A from the substrate. There is therefore a correlation with the data in Fig. 4, where nicking of oligonucleotides B or C at the junction point inhibits the displacement of oligonucleotide A.

Initiation of unwinding of duplex Y Junctions is sequence dependent. The data above indicate that DNA base sequence is a major determinant in the efficiency of D10 Y-junction unwinding. Without *a priori* knowledge of D10 sequence requirements a corollary to this observation is that the initial choice of substrate sequence was fortuitous in terms of revealing its ability to be unwound. We therefore altered Y20 in two ways to test whether sequence alterations alter its susceptibility to D10-mediated unwinding. The alterations made were limited to the 7 base pairs of each fork arm closest to the junction point where DEPC interference was most apparent in helicase assays. To generate the oligonucleotide sequences for substrate Y20', as illustrated in Fig. 7a, the sequence of the 3 base pairs at the junction point of each dsDNA arm of Y20 ('section 1') was changed to the sequence of the preceding, counter clockwise, arm *i.e.* a rotational transposition of the 3 bp sequence of each arm in the clockwise direction. To generate the sequences for substrate Y20'', the nucleotide base pair sequence at positions 4–7 of each oligonucleotide ('section 2') were transposed similarly. Such sequence transformations had only a minimal impact on ATPase activity with only Y20'' showing a slightly reduced (~30%) ability to stimulate the rate of D10-catalysed ATP hydrolysis (Fig. 7b).

Next, each oligonucleotide of the substrates was labelled individually in order to determine how they are processed in helicase assays (Fig. 7c). For Y20', lanes 1–18 and control reactions, the sequence alteration at the branch point shifted the preference for displacement predominantly from the context of oligo A to oligo B. In addition, the other oligonucleotides were displaced from the substrate but with reduced efficiency. Overall, Y20' was unwound with similar efficiency to Y20 (lanes 19–23). In contrast, the sequence transformation in substrate Y20'' resulted in complete inhibition of D10 catalysed unwinding. Thus, since near complete unwinding

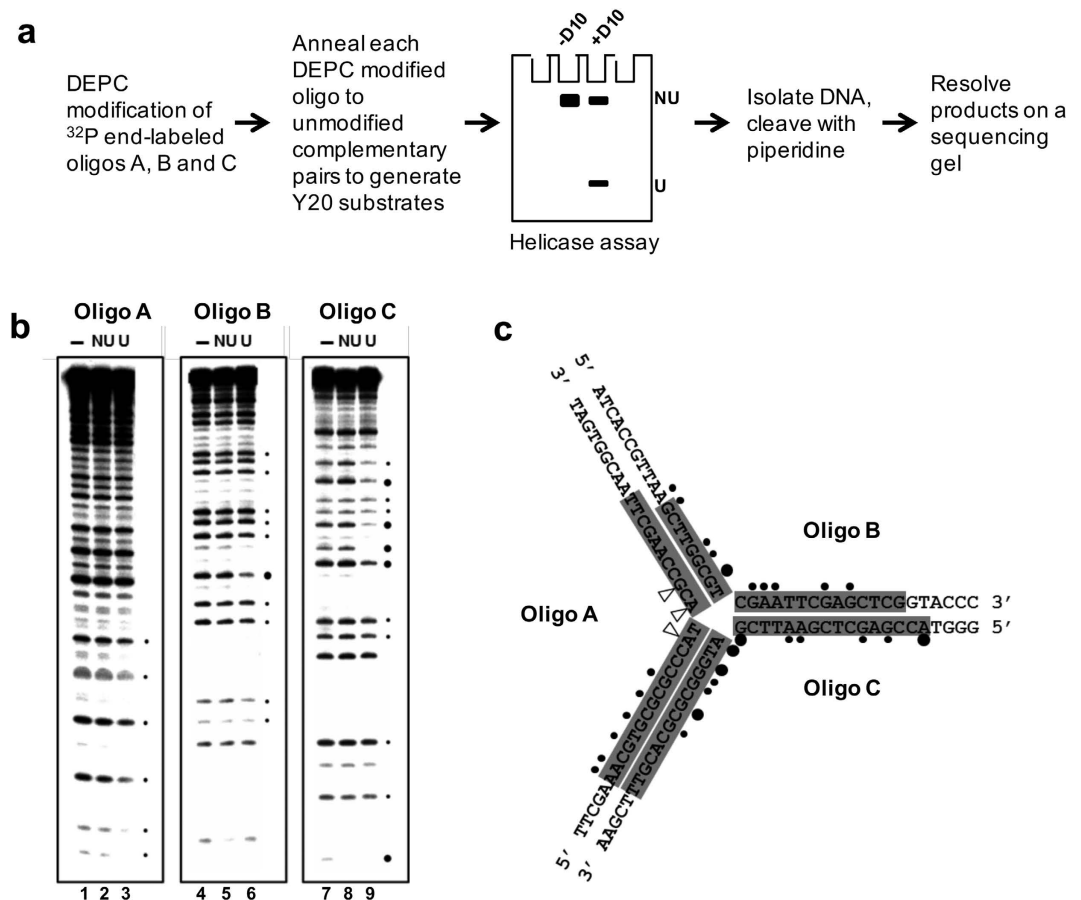


Figure 6. DEPC interference analysis of the unwinding of Y20 by D10. (a) Schematic diagram of the experimental procedure (NU = substrate not unwound and U = unwound substrate). (b) The helicase reactions were performed with D10 and one each of the three strands of substrates Y20 was ^{32}P end-labelled and DEPC-modified. Positions of interference are indicated (circles). (c) The OH protection is shaded in grey and the positions of modification-interference within the Y20 substrate indicated (black dots, interference; small symbol, less than 40% change; large symbol, 40–70% change).

of substrate Y20 is achieved in less than 5 minutes (Fig. 4a) and no unwinding of substrate Y20'' was observed in 20 minutes, small sequence alterations have very large effects on substrate unwinding. There is no correlation between oligonucleotide GC base content in the first 6 residues either side of the fork junction and strand displacement. For example, oligonucleotide A is efficiently and exclusively displaced from substrate Y20 and in oligonucleotide A four of the six nucleotides are G or C residues in each of the first six nucleotides either side of the junction point (eight in total) while in oligonucleotides B and C there are a total of six G or C residues, also considering the six nucleotides either side of the junction point. Thus, reduced thermal stability is unlikely to account for selective displacement of oligonucleotide A from Y20. Also, although there are two A:T base pairs at the junction formed by oligonucleotide A and only one for oligonucleotides B and C it is known that each of the first bases at the branch point in such three-way junctions are unpaired²⁹ and therefore unlikely to make any contribution to junction stability and selective unwinding. This is confirmed by the complete failure of D10 to displace oligonucleotide A'' from substrate Y'', where the two A:T base pairs at the fork junction point are maintained.

Furthermore, in the absence of ATP/Mg²⁺, all three substrates (Y20, Y20' and Y20'') were bound by D10 to similar extents and three principal complexes (C1–3) were observed when all substrate was bound by protein, as shown in Fig. 7d lanes 2, 9 and 16. D10 binding to each Y-junction substrate demonstrated very similar sensitivity to the addition of increasing amounts of non-specific competitor DNA poly d(AT), indicating a near identical D10 binding affinity for all substrates.

Discussion

Like its closest characterised homologue T4 UvsW, T5 D10 can unwind synthetic three, and four-way branched dsDNA substrates by branch migration. However, unlike UvsW and the other known branch migration enzymes including *E. coli* RecG³¹ and RuvAB³², helicase action is influenced by the sequence of the branched dsDNA substrates. Substrate sequence had a significant effect on the ability of D10 to unwind simple Y-shaped molecules with two ssDNA tails (Fig. 2) as well as how branched substrates with three and four dsDNA arms were processed. Unlike four-way dsDNA junctions, the arms of Y-shaped dsDNA molecules have been shown to behave much like duplex DNA and are relatively insensitive to Mg²⁺ induced structural perturbations due to

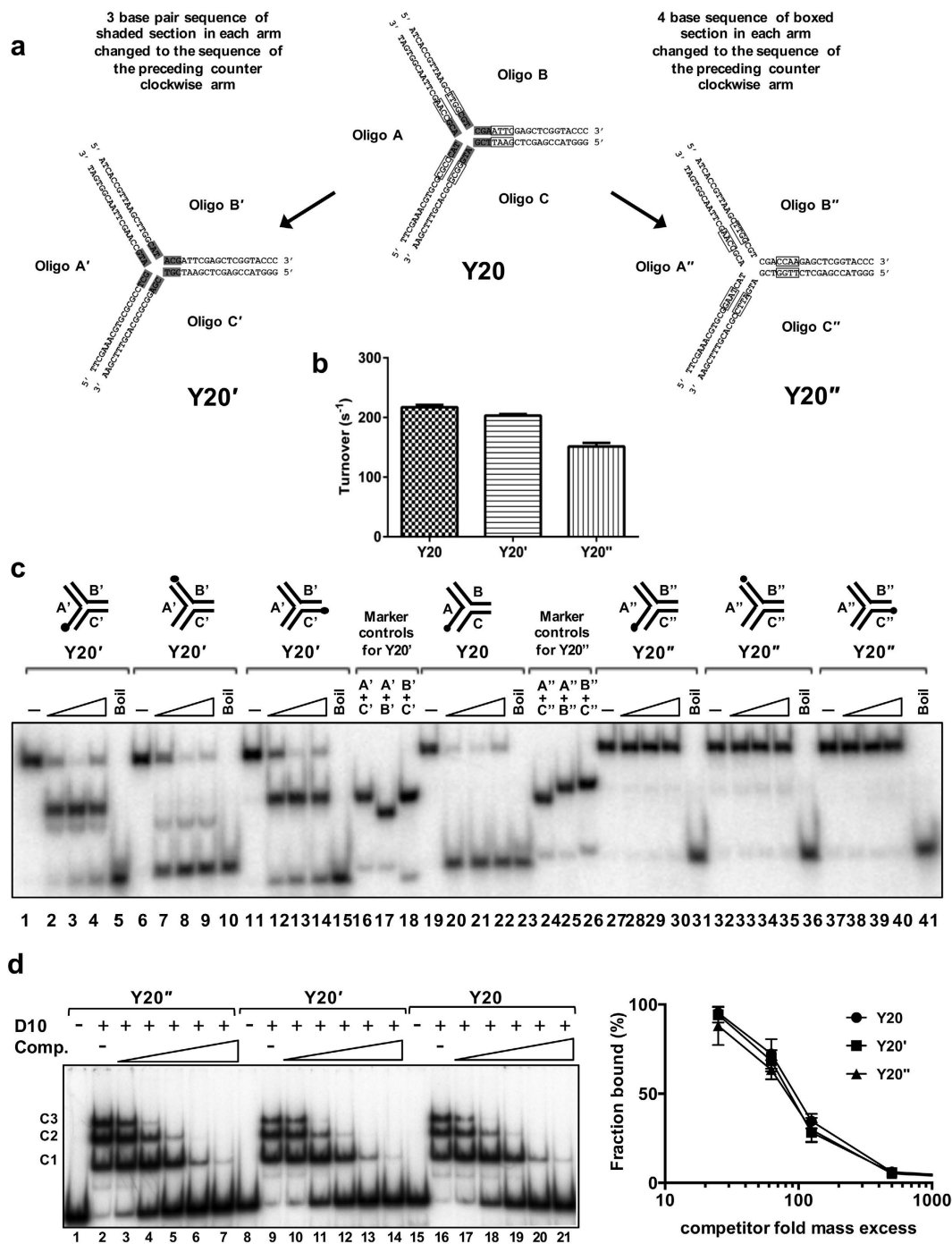


Figure 7. Unwinding and DNA binding of Y20 with sequence alterations. (a) The sequences for generating substrates Y20' and Y20'' were derived by rotating Section 1 (shaded; 3 bp; positions 1–3 from the junction point) and Section 2 (boxed; 4 bp; positions 4–7) of Y20 120° clockwise to adjacent arms. (b) ATPase activity of D10 (5 nM) was determined in the presence of Y20, Y20' or Y20'' (5 nM). (c) D10 displaced all oligonucleotide from Y20', but oligonucleotide B in preference (lanes 1–18; 16–18 are markers for the possible products), but was incapable of unwinding Y20'' (lanes 24–41; lanes 24–26 are markers for the possible products). (d) Gel-shift assay (0.1 nM substrate, 0.4 nM D10) showing D10 binding to Y20'', Y20' and Y20 (lanes 2, 9 and 16 compared to lanes 1, 8 and 15, no protein control (-)). Binding reactions were also performed in the presence of increasing amounts of poly d(AT) competitor (2–200 ng) for each substrate, lanes 3–7 (Y20''), lanes 10–14 (Y20'), and lanes 17–20 (Y20) and the quantified data (n=4, mean and standard deviation) are shown in the graph.

base stacking²⁹. This and the observation that a nick in any one DNA strand at the junction point, that would be expected to relax any conformational constraints induced by metal ions at the junction, does not alter selective strand displacement, reinforcing the notion that D10 is directly sensitive to substrate sequence. Moreover, the

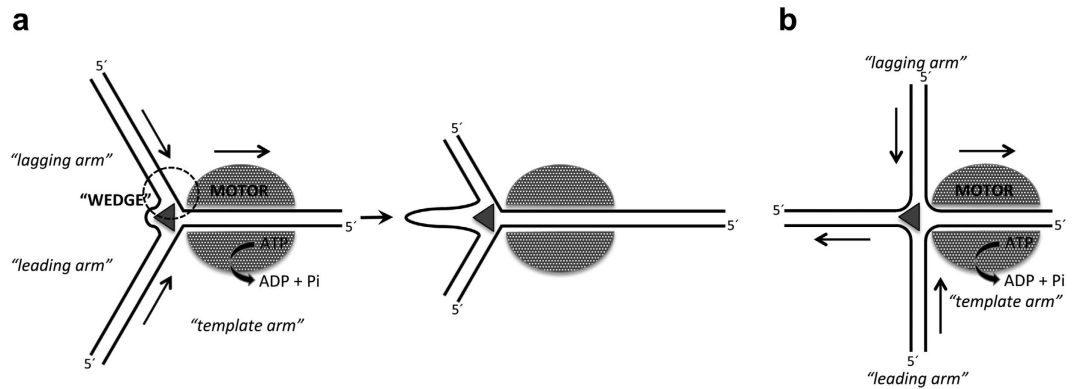


Figure 8. Model for D10 unwinding of branched dsDNA structures. (a) Unwinding of substrate Y20 resembles processing of a stalled replication fork to a “chicken foot” intermediate by RecG. A fork separation “wedge” acts at the junction to unwind nascent leading-, and lagging-strand DNA as the helicase motor moves the “template arm” through the complex. In D10, DNA binding segments of or in proximity to the wedge can sense the sequence context to regulate unwinding (dashed circle). **(b)** D10 can unwind Holliday junction-like substrates that could be established from a stalled replication fork-like substrate as in (a).

effects of breaking the phosphodiester backbone at the junction point are consistent with the notion that productive unwinding is dependent on sequence orientated D10-substrate interactions (see below). In contrast, DNA binding and DNA-dependent ATPase activities were relatively independent of the substrate sequence or insensitive to nicking of the DNA backbone at the junction point. To our knowledge this is the first time that significant sequence-selective initiation of unwinding has been observed for any DNA helicase and branch migration protein.

Primarily, DNA structure rather than base sequence recognition determines where helicases initiate unwinding. Helicases involved in DNA repair such as BLM, WRN^{3,33} and PIF1³⁴ are recruited to branched DNA structures that form during DNA repair. The hexameric replicative helicases are usually loaded on to single-stranded DNA (ssDNA) where their motor domains make DNA base-independent interactions with ssDNA^{6,35}. For *E. coli* DnaB helicase, the ssDNA structure is prepared at *OriC* by the initiator protein DnaA³⁶. For the replicative helicases of SV40 and papillomavirus, large T-antigen and E1 respectively, separate modules for sequence specific origin (*ori*) recognition and helicase action function independently and the initiator binding sequence is separate from the site of helicase binding³⁷. In contrast, the protein sequence alignment of D10 with both UvsW and XPB are not consistent with a truly modular organisation and the putative DNA binding site of UvsW, an arginine/aromatic rich (basic) loop conserved in D10 (Supplementary movie file), is best described as a DNA binding segment within the helicase fold. Furthermore, in D10-three-way dsDNA fork complexes the unwinding junction and sites of close DNA base-protein contact that determine substrate unwinding appear coincident (see below).

In vitro, unwinding of Y-junctions by D10 occurs with a unique polarity that appears to be established by protein-DNA base contacts (Figs 5 and 6). Furthermore, the preferential displacement of one oligonucleotide (“oligo A”) from substrate Y20 resembles the conversion of a three-way stalled replication fork to a Holliday junction via a “chicken foot” intermediate by RecG^{38,39}. As such, the arms of this fork (Y20) can be assigned as either ‘template’, ‘leading’ or ‘lagging’ (Fig. 8). All considered, the data for D10 suggest an operating mechanism similar to RecG, proposed from the atomic structure of the *Thermotoga maritima* protein in complex with a three way DNA junction⁴⁰. The template strand would engage with the motor or translocase module of the complex, and this fits with the observation that DNA strand discontinuity (“nicking”) of either template DNA strand at the junction of Y20 inhibits D10-dependent unwinding (Fig. 4). A DNA strand splitting “wedge” may operate at the fork junction to displace the nascent leading and lagging strand ssDNA, while all dsDNA arms of the fork are in close proximity to protein. We speculate that in D10, the wedge and sequence-sensing residues are likely to be in close proximity. The model of RecG action, and by extension D10, predicts that the enzyme can translocate on dsDNA. Although in the RecG-DNA structure the dsDNA did not extend into the ATPase domain to reveal the motor in operation, the stimulation of ATPase in this type of SF2 helicases by ssDNA is less marked than by dsDNA^{41,42}, and absent in D10 (Fig. 1).

Evaluation of the available structural and biochemical data for SF2 helicases indicate that extensive phosphodiester backbone contacts are necessary for the continuity of the unwinding process while observable nucleobase contacts are not. For example, in the RecG structure aromatic side chains stabilise flipped out bases by simple planar stacking with no indication of base specificity⁴⁰. Similarly, in the RuvA-Holliday junction structure protein-DNA contacts are restricted to the minor groove⁴³. Despite this, pausing, periodic and stepping behaviour that have been observed in single molecule experiments for representative helicases from several superfamilies, not otherwise apparent in ensemble experiments, have been related to sequence context^{44–46}. In each case though, these effects were attributed to the thermodynamic stability of the duplex nucleic acid, rather than direct enzyme-nucleic acid interactions. To date only the vaccinia virus NPH-II helicase involved in aspects of RNA metabolism has been shown to have a distinct bias for a purine-rich tracking strand although the nature of this bias remains unclear⁴⁷.

In marked contrast to the above, our observations indicate that the DNA nucleobases influence D10 unwinding directly for the following reasons: First, minor sequence alterations at the unwinding junction result in profound changes in substrate unwinding ability while DNA binding and DNA dependent ATPase are relatively unaffected, while there is no correlation between GC content and the efficiency with which a strand is displaced from a test substrate. Second, as discussed previously, the combination of OH⁻ protection, DEPC interference and the effects of DNA strand nicking reveal a stereo-specific mode of DNA interaction that relates directly to substrate unwinding specificity. The determinant of this specificity must reside in the DNA base sequence. Protein-nucleobase contacts that determine specific protein-DNA interactions are usually confined to the DNA's major groove⁴⁸ and the DEPC interference assay would indicate close contacts between D10 and purine N7 atoms here.

Although our observations with D10 are based on a strand displacement assay, it is perhaps more likely that direct DNA sequence sensing by D10 (in *cis*) can terminate or pause an already productive unwinding cycle to regulate D10 branch migration. The processing of recombination intermediates by RuvABC and RecBCD is also regulated by specific sequences. In contrast to D10 however, the unwinding action of the RuvB and RecBD motors is regulated, in *trans*, by an auxiliary protein's base-specific recognition of a DNA sequence. The RuvC endonuclease recognises and cleaves Holliday junctions when resolution hotspots are encountered^{49,50}, while RecC interaction with the Chi (χ) sequence resets the operation of the RecBD helicase/endonuclease^{51,52}. Similarly, the *Bacillus subtilis* AddAB helicase/nuclease, which like RecBCD is involved in DNA break processing, is regulated by the AddB subunit. In this case AddB is responsible for Chi recognition and is structurally related to the AddA SF1 helicase but catalytically inactive. Interestingly, the ssDNA-binding groove in AddB is highly modified to provide the specificity for Chi binding through base interactions⁵³. Thus, in the SF2 helicase D10 it is plausible that the helicase's ssDNA binding groove can provide base sensing without loss of the motor function.

The replication apparatus of bacteriophage T5 has not been widely studied despite its prodigious replicative capacity²². The previously reported T5 D2 helicase has the unusual properties of possessing a bi-polar unwinding activity and the ability of non-hydrolysable adenine nucleotides to support limited 3'-5' helicase action²⁵. Although the roles of D10 and D2 in T5 replication are unclear, we can speculate that for D10 at least, the sequence and functional similarities with UvsW contribute to the replication efficiency of T5 through RDR.

Genes capable of encoding D10 homologs are present in the genomes of viruses from eukaryotic and prokaryotic hosts as well as in archaeobacteria such as the *A. fulgidus* Xpb helicase which is involved in replication and nucleotide excision repair⁵⁴. Recently, specific residues of the DNA binding channel of the related XPD helicase have been shown to sense damaged compared to undamaged DNA during excision repair⁵⁵. Thus, the ssDNA-binding groove of SF1 and related SF2 helicases may have evolved a more dynamic range of DNA interacting function over non-specific phosphate backbone contacts, providing base and modified base sensing functions to regulate substrate interactions and processing during catalysis. Furthermore, our studies suggest that DNA sequence-sensing helicases with roles in DNA transcription, replication and recombination are widespread in nature and not solely confined to bacteriophages.

Methods

D10 Constructs. The T5 D10 gene (accession no. YP_006952) was amplified from T5 phage genomic DNA by PCR with *Pfu* DNA polymerase (Promega) using the sense primer (5'-AATTGAATTCTTAAGG TTGTTATATCTAATAAAG-3') and antisense primer (5'-ATTTAAGCTTTTATGAGCTGTTGCCAAATGCA-3'), which included EcoRI and HindIII recognition sites, respectively (underlined). The T5 D10 mutant encoding the R389N substitution was generated by overlapping PCR using these primers together with two additional internal primers (5'-AATGTTCAACGTATTGTC-3' and 5'-AATACGTTGAACATTGCCTGCAAGCTGTTC-3'). The position of the mutated bases are underlined. Each open reading frame (ORF) was cloned into the vector pGEX-KG⁵⁶ and sequence integrity was confirmed using a BigDye Terminator v3.1 Cycle Sequencing Kit and ABI PRISM™ 3730 DNA Analyzer (Applied Biosystems), at the Core Genomics Facility, University of Sheffield Medical School.

Expression and Purification of D10 Protein. Wild-type and R389N D10 glutathione-S-transferase (GST) fusion proteins were expressed in *E. coli* XL1-Blue cells cultured in 2YT media⁵⁷ containing 100 μ g/mL ampicillin at 25 °C for 8 hr following IPTG induction (0.5 mM) at A_{600nm} of 1. Cell pellets were recovered by centrifugation (10,000 \times g, 30 min. at 4 °C) and stored at -80 °C and all the purification steps were performed at 4 °C. Cell pellets were thawed and re-suspended in 3 ml of lysis buffer (25 mM Tris-HCl pH 7.5, 1 M NaCl, 1 mM EDTA, 5 mM DTT, 10% v/v glycerol) per gramme of cells plus 1 mM phenylmethylsulfonylfluoride (PMSF), sonicated and centrifugated at 40,000 \times g for 30 min. A 5% w/v solution of polyethylenimine (pH 8, Sigma-Aldrich, UK), was added to the supernatant to a final concentration of 0.65% w/v and the solution cleared at 25,000 \times g for 5 min. GST-D10 protein was precipitated by addition of ammonium sulphate to 40% saturation and centrifugation at 25,000 \times g for 30 min. The precipitate was dissolved in lysis buffer (1 ml per 10 grams of *E. coli* cells) and incubated with glutathione Sepharose beads (GE Healthcare; 1 ml of beads per 20 grams of cells) for ~18 h. Beads were washed sequentially with 50 bead volumes of lysis buffer, and 50 bead volumes of lysis buffer with 0.3 M NaCl. The GST-D10 protein was eluted with GST elution buffer (25 mM Tris-HCl pH 7.5, 0.3 M NaCl, 1 mM EDTA, 5 mM DTT, 20 mM reduced glutathione, 10% v/v glycerol) and digested with thrombin (~1 unit per g of *E. coli* cells) for ~18 h to cleave off the GST fusion partner. The protein was further purified by cation exchange chromatography (Source S (GE Healthcare)), 10 mM sodium phosphate pH 6.5, 1 mM EDTA, 5 mM DTT, 10% v/v glycerol, 0.2-0.7 M NaCl gradient) and gel filtration (Superdex 75 (GE Healthcare), 20 mM Tris-HCl pH 7.5, 0.3 M NaCl, 1 mM EDTA, 1 mM PMSF, 5 mM DTT, 10% v/v glycerol). Peak fractions were pooled, concentrated,

dispensed into aliquots and stored at -80°C . D10 protein concentration was determined in the presence of 7 M guanidine hydrochloride by UV spectrophotometry using a molar extinction coefficient of $58330\text{ M}^{-1}\text{ cm}^{-1}$.

ATPase Assays. ATPase assays were performed in 20 mM HEPES-NaOH pH 7.5, 120 mM NaCl, 0.1% v/v NP40 alternative (Calbiochem, UK), 0.1 mg/ml BSA, 2 mM DTT, $0.0125\text{ }\mu\text{M}$ [$\gamma\text{-}^{32}\text{P}$]ATP (6000 Ci/mmol), 5 mM MgCl_2 , 5 mM ATP at 22°C for 10 min, unless stated otherwise. The release of radioactive phosphate was measured using the charcoal-binding assay of Iggo and Lane⁵⁸. All data are from a minimum of three repeats and the mean is shown with the standard deviation (SD) delimited by the error bars.

Helicase and electrophoretic mobility shift assays (EMSA). The DNA substrates were constructed by annealing the synthetic oligonucleotides (Table S1 and Figure S7). The oligonucleotides were labeled at the 5' end with T4 polynucleotide kinase and [$\gamma\text{-}^{32}\text{P}$]ATP (6000 Ci/mmol) as indicated in each figure using the protocol previously described³⁴. The labelled substrates were resolved and purified from 8% (19:1) polyacrylamide gels and quantified based on the specific activity of the component oligonucleotides³⁴.

Helicase assays (0.1 nM substrates) were performed in 20 mM HEPES-NaOH pH 7.5, 20 mM NaCl, 0.1% v/v NP40 alternative, 0.1 mg/ml BSA, 2 mM DTT, 5 mM MgCl_2 , 5 mM ATP at 37°C for 20 min and terminated with 6 x stop buffer (120 mM EDTA, 0.6% w/v SDS, 1% w/v bromophenol blue, 60% v/v glycerol). Products were separated on 8% (19:1) polyacrylamide gels containing 0.05% w/v SDS, using 1 x TBE/0.05% w/v SDS running buffer, visualized and quantified by phosphorimaging. Strand annealing assays were performed under the same reaction conditions with or without the addition of ATP as indicated and processed in the same way as helicase assays.

DNA binding reactions (0.1 nM substrates) were performed in 20 mM HEPES-NaOH pH 7.5, 135 mM NaCl, 0.1% v/v NP40 alternative, 0.1 mg/ml BSA, 2 mM DTT, 1 mM EDTA, 10% v/v glycerol at 22°C for 20 min. The binding reactions were resolved on 6% (30:1) polyacrylamide gels in 0.25 x TBE buffer, visualized and quantified as above. Competition assays with poly d(AT) competitor DNA were performed under the same reaction conditions with radiolabeled substrate and competitor DNA mixed before the addition of protein (concentrations indicated in the figure legends). All graphed data shown are from a minimum of three repeats. Data points show the mean and the standard deviation (SD) delimited by the error bars.

Hydroxyl Radical Footprinting. Hydroxyl radical footprinting in solution was carried out essentially as described previously⁵⁹. The binding reactions (50 μl , containing 10 nM of Y20 substrate with one strand ^{32}P end-labelled) were set up as described for the EMSA, except that glycerol was omitted. Following a 20 minute incubation at 22°C , the hydroxyl radical was generated by addition of 0.375 mM sodium ascorbate, 0.0275% w/v H_2O_2 , 1 mM $(\text{NH}_4)_2\text{FeSO}_4\cdot 6\text{H}_2\text{O}$ and 2 mM EDTA for 2 min and quenched with 0.25 volume of 200 mM thiourea. Cleaved products were extracted twice with phenol/chloroform and analyzed on 15% (19:1) polyacrylamide gels containing 8 M urea in 1 x TBE buffer, after adding an equal volume of 98% formamide loading buffer and heating.

DEPC Interference. The Y20 substrates for DEPC interference were prepared by 5' end-labelling one strand with ^{32}P and modifying it with diethylpyrocarbonate (DEPC) essentially as described^{30,60}. Approx. 60 ng of end-labelled DNA was carboxymethylated by adding 4 μl of DEPC in 200 μl of cacodylate buffer (50 mM sodium cacodylate pH 7.0, 1 mM EDTA). After incubation at 37°C for 20 min, the DNA was ethanol precipitated twice and annealed with its complementary oligonucleotides, before gel-purification and quantification as described above. Helicase reactions contained 5 nM substrate and 0.005 nM D10. To generate DEPC interference data for the unwinding reaction, helicase assays were set up so that only a small fraction of the substrate (~17%) was unwound. After electrophoresis, the reaction products were detected by autoradiography and the bands excised from the gel. The DNA was soak-eluted in 1 x TAE buffer (40 mM Tris acetate, 1 mM EDTA) at 4°C overnight and recovered by phenol/chloroform extraction, ethanol precipitation, and cetyltrimethylammonium bromide precipitation. The DNA was then cleaved with piperidine, extracted with butanol and ethanol precipitated. Finally, the products were analyzed on urea-polyacrylamide sequencing gels, as described above.

References

- Singleton, M. R., Dillingham, M. S. & Wigley, D. B. Structure and mechanism of helicases and nucleic acid translocases. *Annu Rev Biochem* **76**, 23–50 (2007).
- Cox, M. M. *et al.* The importance of repairing stalled replication forks. *Nature* **404**, 37–41 (2000).
- Bernstein, K. A., Gangloff, S. & Rothstein, R. The RecQ DNA helicases in DNA repair. *Annu Rev Genet* **44**, 393–417 (2010).
- Itsathitphaisarn, O., Wing, R. A., Eliason, W. K., Wang, J. & Steitz, T. A. The hexameric helicase DnaB adopts a nonplanar conformation during translocation. *Cell* **151**, 267–77 (2012).
- Pyle, A. M. Translocation and unwinding mechanisms of RNA and DNA helicases. *Annu Rev Biophys* **37**, 317–36 (2008).
- Enemark, E. J. & Joshua-Tor, L. Mechanism of DNA translocation in a replicative hexameric helicase. *Nature* **442**, 270–5 (2006).
- Hamdan, S. M. & Richardson, C. C. Motors, switches, and contacts in the replisome. *Annu Rev Biochem* **78**, 205–43 (2009).
- Dudas, K. C. & Kreuzer, K. N. UvsW protein regulates bacteriophage T4 origin-dependent replication by unwinding R-loops. *Mol Cell Biol* **21**, 2706–15 (2001).
- Jones, C. E., Mueser, T. C., Dudas, K. C., Kreuzer, K. N. & Nossal, N. G. Bacteriophage T4 gene 41 helicase and gene 59 helicase-loading protein: a versatile couple with roles in replication and recombination. *Proc Natl Acad Sci USA* **98**, 8312–8 (2001).
- Mosig, G. Recombination and recombination-dependent DNA replication in bacteriophage T4. *Annu Rev Genet* **32**, 379–413 (1998).
- Dong, F., Gogol, E. P. & von Hippel, P. H. The phage T4-coded DNA replication helicase (gp41) forms a hexamer upon activation by nucleoside triphosphate. *J Biol Chem* **270**, 7462–73 (1995).
- Venkatesan, M., Silver, L. L. & Nossal, N. G. Bacteriophage T4 gene 41 protein, required for the synthesis of RNA primers, is also a DNA helicase. *J Biol Chem* **257**, 12426–34 (1982).

13. Carles-Kinch, K., George, J. W. & Kreuzer, K. N. Bacteriophage T4 UvsW protein is a helicase involved in recombination, repair and the regulation of DNA replication origins. *EMBO J* **16**, 4142–51 (1997).
14. Long, D. T. & Kreuzer, K. N. Fork regression is an active helicase-driven pathway in bacteriophage T4. *EMBO Rep* **10**, 394–9 (2009).
15. Webb, M. R., Plank, J. L., Long, D. T., Hsieh, T. S. & Kreuzer, K. N. The phage T4 protein UvsW drives Holliday junction branch migration. *J Biol Chem* **282**, 34401–11 (2007).
16. Sakakibara, N., Chen, D. & McBride, A. A. Papillomaviruses use recombination-dependent replication to vegetatively amplify their genomes in differentiated cells. *PLoS Pathog* **9**, e1003321 (2013).
17. McCorquodale, D. J. & Warner, H. R. *The Bacteriophages*. ed Calendar, R. 439–475 (Plenum Press, New York, 1988).
18. Sayers, J. R. *The Bacteriophages*. ed Calendar, R. 268–276 (Oxford University Press, New York, 2005).
19. Constantinou, A., Voelkel-Meiman, K., Sternglanz, R., McCorquodale, M. M. & McCorquodale, D. J. Involvement of host DNA gyrase in growth of bacteriophage T5. *J Virol* **57**, 875–82 (1986).
20. Gentz, R. & Bujard, H. Promoters recognized by *Escherichia coli* RNA polymerase selected by function: highly efficient promoters from bacteriophage T5. *J Bacteriol* **164**, 70–7 (1985).
21. Wang, J. *et al.* Complete genome sequence of bacteriophage T5. *Virology* **332**, 45–65 (2005).
22. Heusterspreute, M., Ha-Thi, V., Tournis-Gamble, S. & Davison, J. The first-step transfer-DNA injection-stop signal of bacteriophage T5. *Gene* **52**, 155–64 (1987).
23. Chatterjee, D. K., Fujimura, R. K., Campbell, J. H. & Gerard, G. F. Cloning and overexpression of the gene encoding bacteriophage T5 DNA polymerase. *Gene* **97**, 13–9 (1991).
24. Sayers, J. R. & Eckstein, F. Properties of overexpressed phage T5 D15 exonuclease. Similarities with *Escherichia coli* DNA polymerase I 5'-3' exonuclease. *J Biol Chem* **265**, 18311–7 (1990).
25. Wong, I. N., Sayers, J. R. & Sanders, C. M. Characterization of an unusual bipolar helicase encoded by bacteriophage T5. *Nucleic Acids Res* **41**, 4587–600 (2013).
26. AlMalki, F. A., Flemming, C. S., Zhang, J., Feng, M., Sedelnikova, S. E., Ceska, T., Rafferty, J. B., Sayers, J. R. & Artymiuk, P. J. Direct observation of DNA threading in flap endonuclease complexes. *Nature Structural & Molecular Biology*, **23**, 640–6 (2016).
27. Kaliman, A. V., Kryukov, V. M. & Bayev, A. A. The nucleotide sequence of the region of bacteriophage T5 early genes D10-D15. *Nucleic Acids Res* **16**, 10353–4 (1988).
28. Kerr, I. D. *et al.* Crystallographic and NMR analyses of UvsW and UvsW.1 from bacteriophage T4. *J Biol Chem* **282**, 34392–400 (2007).
29. Sabir, T. *et al.* Branchpoint expansion in a fully complementary three-way DNA junction. *J Am Chem Soc* **134**, 6280–5 (2012).
30. Sturm, R., Baumruker, T., Franza, B. R., Jr. & Herr, W. A 100-kD HeLa cell octamer binding protein (OBP100) interacts differently with two separate octamer-related sequences within the SV40 enhancer. *Genes Dev* **1**, 1147–60 (1987).
31. Tsaneva, I. R., Muller, B. & West, S. C. RuvA and RuvB proteins of *Escherichia coli* exhibit DNA helicase activity *in vitro*. *Proc Natl Acad Sci USA* **90**, 1315–9 (1993).
32. Whitby, M. C., Vincent, S. D. & Lloyd, R. G. Branch migration of Holliday junctions: identification of RecG protein as a junction specific DNA helicase. *EMBO J* **13**, 5220–8 (1994).
33. Mohaghegh, P., Karow, J. K., Brosh, R. M., Jr., Bohr, V. A. & Hickson, I. D. The Bloom's and Werner's syndrome proteins are DNA structure-specific helicases. *Nucleic Acids Res* **29**, 2843–9 (2001).
34. George, T. *et al.* Human Pif1 helicase unwinds synthetic DNA structures resembling stalled DNA replication forks. *Nucleic Acids Res* **37**, 6491–502 (2009).
35. Soultanas, P. Loading mechanisms of ring helicases at replication origins. *Mol Microbiol* **84**, 6–16 (2012).
36. Bramhill, D. & Kornberg, A. Duplex opening by DnaA protein at novel sequences in initiation of replication at the origin of the *E. coli* chromosome. *Cell* **52**, 743–55 (1988).
37. Gai, D., Chang, Y. P. & Chen, X. S. Origin DNA melting and unwinding in DNA replication. *Curr Opin Struct Biol* **20**, 756–62 (2010).
38. McGlynn, P. & Lloyd, R. G. Modulation of RNA polymerase by (p)ppGpp reveals a RecG-dependent mechanism for replication fork progression. *Cell* **101**, 35–45 (2000).
39. McGlynn, P. & Lloyd, R. G. Rescue of stalled replication forks by RecG: simultaneous translocation on the leading and lagging strand templates supports an active DNA unwinding model of fork reversal and Holliday junction formation. *Proc Natl Acad Sci USA* **98**, 8227–34 (2001).
40. Singleton, M. R., Scaife, S. & Wigley, D. B. Structural analysis of DNA replication fork reversal by RecG. *Cell* **107**, 79–89 (2001).
41. Preugschat, F., Averett, D. R., Clarke, B. E. & Porter, D. J. A steady-state and pre-steady-state kinetic analysis of the NTPase activity associated with the hepatitis C virus NS3 helicase domain. *J Biol Chem* **271**, 24449–57 (1996).
42. Whitby, M. C. & Lloyd, R. G. Targeting Holliday junctions by the RecG branch migration protein of *Escherichia coli*. *J Biol Chem* **273**, 19729–39 (1998).
43. Ariyoshi, M., Nishino, T., Iwasaki, H., Shinagawa, H. & Morikawa, K. Crystal structure of the holliday junction DNA in complex with a single RuvA tetramer. *Proc Natl Acad Sci USA* **97**, 8257–62 (2000).
44. Cheng, W., Dumont, S., Tinoco, I., Jr. & Bustamante, C. NS3 helicase actively separates RNA strands and senses sequence barriers ahead of the opening fork. *Proc Natl Acad Sci USA* **104**, 13954–9 (2007).
45. Donmez, I., Rajagopal, V., Jeong, Y. J. & Patel, S. S. Nucleic acid unwinding by hepatitis C virus and bacteriophage T7 helicases is sensitive to base pair stability. *J Biol Chem* **282**, 21116–23 (2007).
46. Qi, Z., Pugh, R. A., Spies, M. & Chemla, Y. R. Sequence-dependent base pair stepping dynamics in XPD helicase unwinding. *Elife* **2**, e00334 (2013).
47. Taylor, S. D., Solem, A., Kawaoka, J. & Pyle, A. M. The NPH-II helicase displays efficient DNA x RNA helicase activity and a pronounced purine sequence bias. *J Biol Chem* **285**, 11692–703 (2010).
48. Rohs, R. *et al.* Origins of specificity in protein-DNA recognition. *Annu Rev Biochem* **79**, 233–69 (2010).
49. Shah, R., Bennett, R. J. & West, S. C. Genetic recombination in *E. coli*: RuvC protein cleaves Holliday junctions at resolution hotspots *in vitro*. *Cell* **79**, 853–64 (1994).
50. Shah, R., Cosstick, R. & West, S. C. The RuvC protein dimer resolves Holliday junctions by a dual incision mechanism that involves base-specific contacts. *EMBO J* **16**, 1464–72 (1997).
51. Dillingham, M. S. & Kowalczykowski, S. C. RecBCD enzyme and the repair of double-stranded DNA breaks. *Microbiol Mol Biol Rev* **72**, 642–71, Table of Contents (2008).
52. Taylor, A. F. & Smith, G. R. Regulation of homologous recombination: Chi inactivates RecBCD enzyme by disassembly of the three subunits. *Genes Dev* **13**, 890–900 (1999).
53. Krajewski, W. W. *et al.* Structural basis for translocation by AddAB helicase-nuclease and its arrest at chi sites. *Nature* **508**, 416–9 (2014).
54. Fan, L. *et al.* Conserved XPB core structure and motifs for DNA unwinding: implications for pathway selection of transcription or excision repair. *Mol Cell* **22**, 27–37 (2006).
55. Mathieu, N., Kaczmarek, N., Ruthemann, P., Luch, A. & Naegeli, H. DNA quality control by a lesion sensor pocket of the xeroderma pigmentosum group D helicase subunit of TFIIH. *Curr Biol* **23**, 204–12 (2013).
56. Guan, K. L. & Dixon, J. E. Eukaryotic proteins expressed in *Escherichia coli*: an improved thrombin cleavage and purification procedure of fusion proteins with glutathione S-transferase. *Anal Biochem* **192**, 262–7 (1991).

57. Sambrook, J. & Russell D. W. *Molecular cloning - a laboratory manual* (Cold Spring Harbor Laboratory Press, Cold Spring Harbor, NY, 2001).
58. Iggo, R. D. & Lane, D. P. Nuclear protein p68 is an RNA-dependent ATPase. *EMBO J* **8**, 1827–31 (1989).
59. Dixon, W. J. *et al.* Hydroxyl radical footprinting. *Methods Enzymol* **208**, 380–413 (1991).
60. Chen, G. & Stenlund, A. Characterization of the DNA-binding domain of the bovine papillomavirus replication initiator E1. *J Virol* **72**, 2567–76 (1998).

Acknowledgements

This work was supported by a Sheffield University Doctoral Fellowship to I.N.W. and benefitted from infrastructure provided by the Biotechnology and Biology Research Council ref. numbers BB/F014732/1 and 50/BB/19466 (awarded to J.R.S.)

Author Contributions

C.M.S. and J.R.S. conceived and coordinated the study. C.M.S., I.N.W. and J.R.S. designed experiments, analysed data, interpreted data and wrote the paper. I.N.W. and C.M.S. performed experiments. All authors reviewed the results and approved the final version of the manuscript.

Additional Information

Supplementary information accompanies this paper at <http://www.nature.com/srep>

Competing financial interests: The authors declare no competing financial interests.

How to cite this article: Wong, I. N. *et al.* Bacteriophage T5 gene D10 encodes a branch-migration protein. *Sci. Rep.* **6**, 39414; doi: 10.1038/srep39414 (2016).

Publisher's note: Springer Nature remains neutral with regard to jurisdictional claims in published maps and institutional affiliations.



This work is licensed under a Creative Commons Attribution 4.0 International License. The images or other third party material in this article are included in the article's Creative Commons license, unless indicated otherwise in the credit line; if the material is not included under the Creative Commons license, users will need to obtain permission from the license holder to reproduce the material. To view a copy of this license, visit <http://creativecommons.org/licenses/by/4.0/>

© The Author(s) 2016